PTC

ISIJ International, Vol. 44 (2004), No. 11, pp. 1902–1910

Cold Swaging, Recovery and Recrystallization of Oligocrystalline INCOLOY MA 956—Part II: Annealed State

Marcio Ferreira HUPALO, Angelo Fernando PADILHA, Hugo Ricardo Zschommler SANDIM[1)] and Andrea Madeira KLIAUGA[2)]

Departamento de Engenharia Metalúrgica e de Materiais, Escola Politécnica, Universidade de São Paulo, São Paulo, SP, 05508-900, Brazil. E-mail: padilha@usp.br 1) Departamento de Engenharia de Materiais, Faculdade de Engenharia Química de Lorena, P.O.Box 116, Lorena, SP, 12600-970, Brazil. 2) Departamento de Engenharia de Materiais, Universidade Federal de São Carlos, Rodovia Washington Luís (SP-310), km 235, São Carlos, SP, 13565-905, Brazil.

(*Received on May 17, 2004; accepted in final form on August 10, 2004*)

The combination of a coarse-grained structure (oligocrystalline material), a strong initial texture, and the presence of fine particles make ODS superalloys like INCOLOY MA 956 very interesting materials for recrystallization studies. In the present paper, we have investigated the annealing behavior of the MA 956 alloy deformed by cold swaging to reductions of 20, 47, 61, and 72 % followed by annealing at temperatures ranging from 600 to 1 450°C. Light optical, scanning, and transmission electron microscopy were used to follow the microstructural changes upon annealing. Orientations of individual grains as well as microtexture were determined by electron backscatter diffraction (EBSD). Recrystallization texture was determined by X-ray diffraction (XRD). The isothermal softening kinetics curves were determined for all samples. Discontinuous recrystallization and extended recovery are responsible for the softening of this alloy. The Johnson-Mehl-Avrami-Kolmogorov (JMAK) model was used to test our experimental data. The Avrami exponents ($0.26 \leq n \leq 0.48$) showed substantially smaller values than those predicted theoretically. This can be attributed to concurrent recovery and to a non-random distribution of recrystallization nuclei.

KEY WORDS: INCOLOY MA 956; oligocrystalline; microstructure; recovery; recrystallization; texture; particle pinning; EBSD.

1. Introduction

Understanding the annealing behavior of particle-containing materials is essential to control their final microstructure and, therefore, enabling the development of new alloys for applications at high temperatures. In an earlier paper (Part I) we have performed the microstructural characterization of MA 956 alloy in the as-received and deformed conditions. A fairly homogeneous and closely spaced dispersion of particles is found throughout the microstructure of this ODS superalloy. It is very well known that this type of microstructure is very effective for pinning low and high angle boundaries during their migration (Zener pinning). Furthermore, the combination of a coarse-grained microstructure, a strong initial texture, and the presence of a fine dispersion of non-deformable particles make this alloy a very interesting material for recrystallization studies. As far as we concern, most of the literature[1-5)] reports the recrystallization behavior in P/M ODS alloys with regard to aspects associated to the primary recrystallization of these materials from the deformed structure (as-milled and as-extruded powders upon hot consolidation) and further secondary recrystallization to obtain a coarse ing. The microstructure of this superalloy in the annealed state was characterized with aid of several techniques including light optical (LOM), scanning and transmission electron microscopy (SEM and TEM), and Vickers microhardness testing. Texture and microtexture measurements of selected regions were performed using conventional X-ray diffraction procedures (XRD) and electron backscatter diffraction (EBSD), respectively. As a first approach we have used the well-known Johnson-Mehl-Avrami-Kolmogorov (JMAK) model to investigate the recrystallization kinetics of this alloy. The main results of this microstructural characterization will be presented and discussed.

2. Experimental Procedure

A bar of 30 mm diameter was cold deformed in a four-die rotary swaging machine to reductions of 20, 47, 61 and 72 % (in area). After cold swaging, the specimens were annealed in temperatures ranging from 600 to 1 450°C from 2 to 120 min. Samples for metallographic examination were cut from the transverse orientation relative to bar axis. They were ground and polished using conventional techniques. Chemical etching of the polished sections was performed

10406

croscopy, and electron backscatter diffraction. Further experimental details were presented in Part I. The microstructure of annealed samples was observed in a Philips XL-30 scanning electron microscope operating at 10 kV in the backscattered electrons mode to reveal orientation contrast. The recrystallization texture was determined by the X-ray diffraction technique using a texture goniometer with a Mo Kα1 (λ=0.07093 nm) radiation. Vickers hardness tests were made in annealed samples using a Buehler Micromet 2004 microindenter with a load of 300 g (15 measurements per sample). The recrystallized volume fraction (V_V) was determined by the linear intercept method (20 fields per sample, in average), following ASTM E562-02, with aid of a light optical microscope.

3. Results and Discussion

3.1. Softening Kinetics

Figure 1 shows the isothermal softening kinetics curves for MA 956 deformed to reductions of 20, 47, 61, and 72% and further annealed in the range 600–1 200°C. We have used the following criterion for microhardness testing of annealed specimens: only "recovered" (non-recrystallized) regions were indented.*[1] The static softening kinetics expressed by hardness *versus* time isothermal plots displays a classical behavior. It is noticeable that the softening rate is very fast in the first 20 min of annealing, however, after 40 min hardness is levelled remaining nearly unchanged for longer times. The amount of softening was found to depend on the annealing temperature; however, this effect is more pronounced for the most deformed samples. The relative standard deviation (RSD) was lower than 5%. The softening behavior was also studied by means of the fractional softening (X) calculated by the following equation:

$$X(\%)=\left(\frac{H_D-H_A}{H_D-H_i}\right)\times 100 \quad \text{.....(1)}$$

where H_i, H_D and H_A are the hardness for the initial, deformed and annealed states, respectively. The fractional softening (X) values calculated from Eq. (1) showed extremely larger values in comparison to those commonly found in the literature to structures softened by recovery. In most cases the amount of softening in our samples has exceeded 70% reaching up to 90% for the most severe annealing condition. For example, Belyakov and co-workers[7] studied the recovery of oxide-bearing steels contend comparable dispersions of iron-oxide particles (in amount and size). For samples deformed between 30 and 85% reduction in compression, they have found that the softening fraction due to recovery was lower than 40%. However, it must be noted that the maximum temperature and annealing time used by those authors were limited to 800°C and 1 h, respectively.

3.2. Microstructural Characterization

The effect of annealing on the substructure of this alloy is clearly demonstrated in the electron transmission micro-

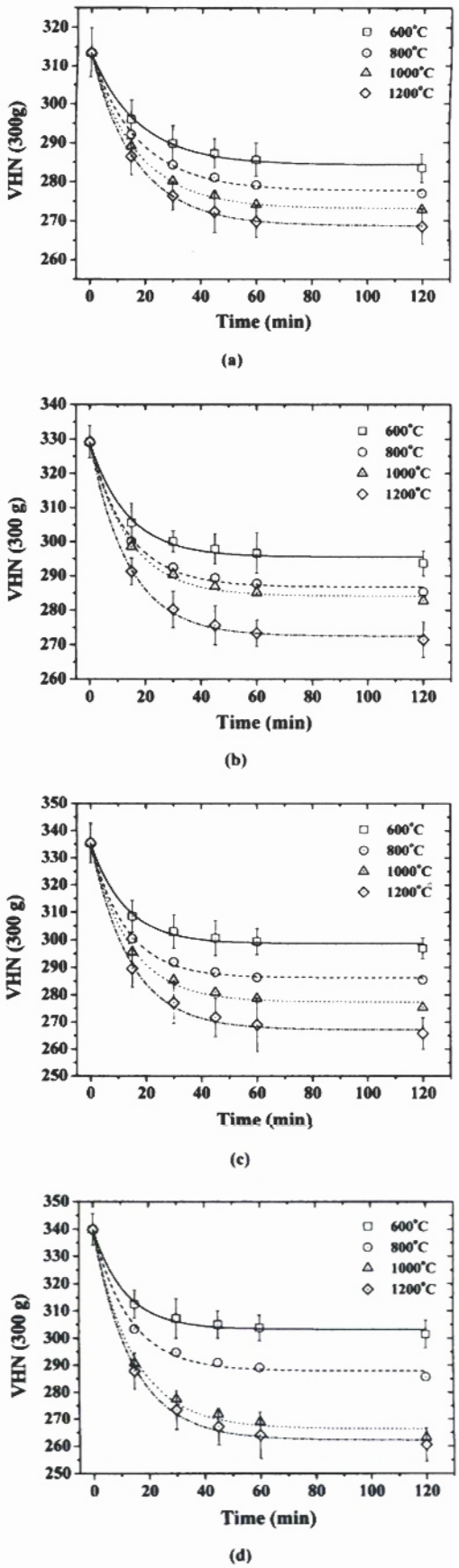

Fig. 1. Softening kinetics for MA 956 alloy deformed by cold swaging to the following reductions: a) 20%; b) 47%; c) 61%; d) 72%.

graphs shown in **Fig. 2**. These micrographs were taken from a sample deformed to 47% reduction and further annealed at 800°C for 1 h. They reveal the presence of a complex microstructure consisting of subgrains and very small grains (sizing less than 1 μm), besides particles. These tiny recrystallized grains cannot be resolved by light optical microscopy; however, they might explain why softening kinetics is so pronounced upon annealing. Recovery itself cannot explain the large amount of softening experienced by this superalloy.

Nevertheless, large grains can be resolved by LOM and become distinguishable in the microstructure. At the beginning of "recrystallization" they are mostly found at deformation heterogeneities and also at grain boundary regions. **Figure 3** shows SEM micrographs depicting examples of preferential recrystallization within deformation bands. The large curvature associated to these regions and the higher amount of stored dislocations might explain why recrystallization is favored at grain boundaries and, in some cases, is virtually suppressed within grains. Electron channeling contrast maps allow the identification of details of the microstructure. In the micrographs displayed in Fig. 3 one can observe that are clear changes in orientation from one region to another (different gray tones).

The presence of large deformation heterogeneities at large particles (>500 nm) might contribute for the nucleation of new grains (particle stimulated nucleation or PSN), however, PSN was observed to occur in a very few cases as the one shown in **Fig. 4**.

The shape of subgrains depends on the extent of pinning exerted by particles, as clear shown in **Fig. 5**. Pinning of low-angle boundaries by arrays of particles is evident. The dislocation density inside the subgrains is much lower as a result of recovery. It was not possible to resolve details of

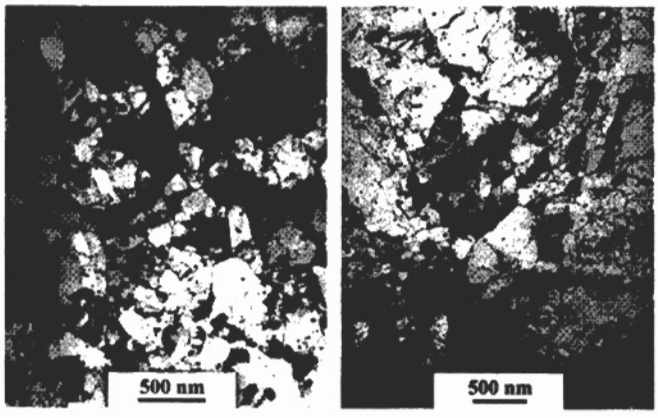

Fig. 2. Recovered substructures in MA 956 sample deformed to 47% reduction and annealed at 800°C for 1 h (TEM, bright field).

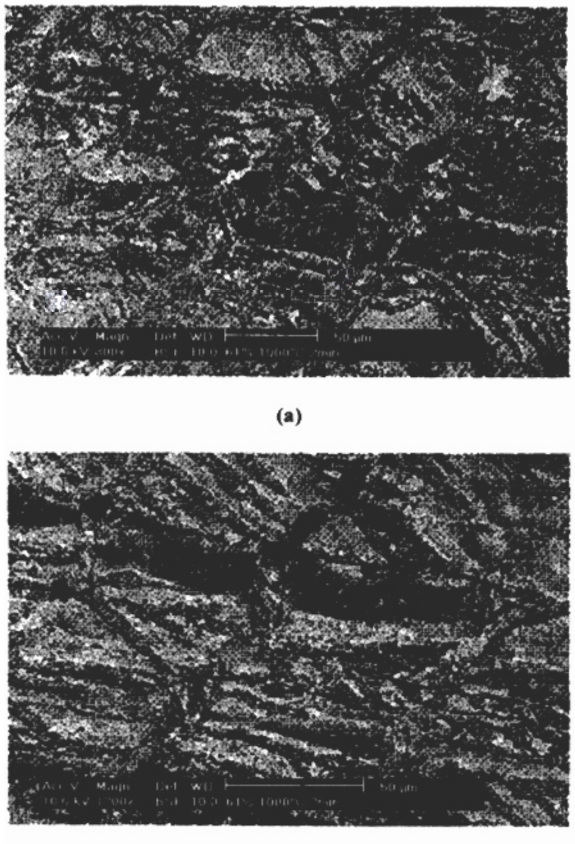

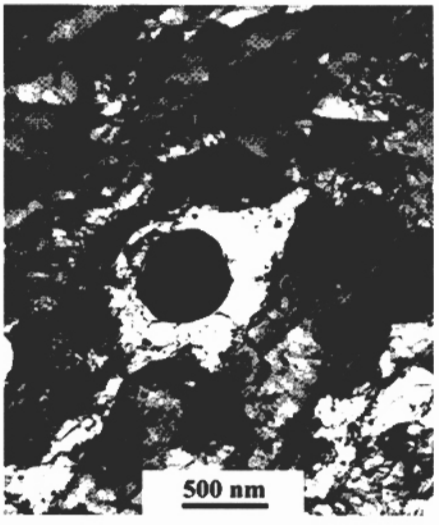

Fig. 4. Particle-stimulated nucleation (PSN) in a sample deformed to 72% reduction and annealed at 800°C for 1 h (TEM, bright field).

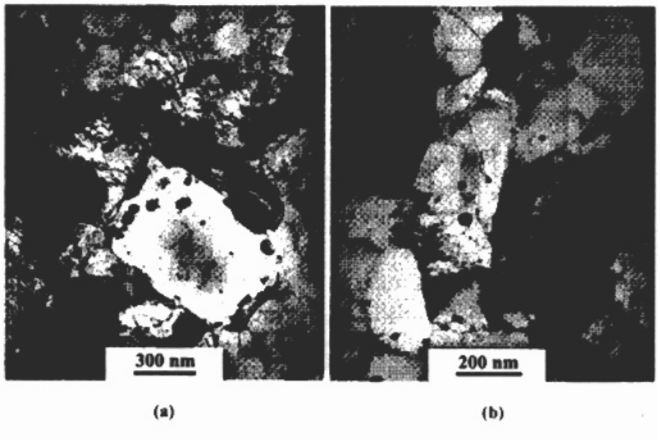

Fig. 5. TEM micrographs (bright field) showing details of substructures in a sample deformed to 47% reduction and

the dislocation structure in the subgrain boundaries. At a first sight, these subgrains boundaries appear to be less organized than the structures usually found in pure high-SFE metals.

Examples of recrystallized grains observed by TEM in a sample deformed to 72% reduction and annealed at 800°C for 1 h are given in **Fig. 6**. Dislocation-free volumes limited by high-angle boundaries are clearly shown in these micrographs. The surrounding structures and the dispersion of particles within the new grains are also noticeable. These grains have gained the necessary mobility to grow towards the recovered substructure, *i.e.*, Zener pinning was ineffective to pin their high-angle boundaries.

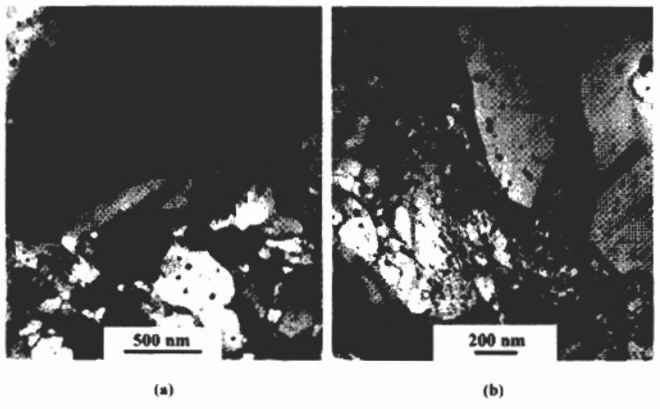

Fig. 6. TEM micrographs (bright field) showing recrystallized grains and surrounding structures in a sample deformed to 72% reduction and annealed at 800°C for 1 h.

At this point of discussion, we must stress that the microstructure of this ODS superalloy in the annealed state consists of grains large enough to be resolved by LOM and very small grains (usually below 1 μm in size) interspersed in a particle-stabilized subgrain structure. The latter is typically found in the "recovered regions" of the annealed samples.

The results of the qualitative description of microstructures observed in the transverse sections after annealing are presented in **Tables 1–4** as a function of time and temperature for the respective reductions. These microstructures are classified according to their recrystallized volume fraction (V_V). The criterion for such classification was the presence of recrystallized grains (or not) using light optical microscopy (LOM). Accordingly, in recovered (RV) specimens $V_V=0$; $0<V_V<0.95$ in partially recrystallized (PR); and $V_V \geq 0.95$ in totally recrystallized (TR) ones. As clearly demonstrated in Tables 1–4, the recrystallized volume fraction of grains resolved by LOM is larger for higher annealing temperatures and for longer annealing times. It should be noted that even for the sample deformed to 72% reduction and annealed at 1 450°C for 1 h there are small regions where "recrystallization" is absent.

The recrystallized microstructure was found to be very

Table 1. Annealed microstructures and recrystallized volume fractions (V_V) for samples deformed to 20% reduction.

Time	Annealing temperature (°C)										
(min)	600	700	800	900	1000	1100	1200	1300	1350	1400	1450
2	RV	-	RV	-	RV	-	RV	-	-	-	-
5	RV	-	RV	-	RV	-	RV	-	-	-	-
10	RV	-	RV	-	RV	-	RV	-	-	-	-
15	RV	-	PR < 5%	-	PR < 5%	-	PR < 5%	-	-	-	-
30	RV	-	PR < 5%	-	PR < 5%	-	PR < 5%	-	-	-	-
45	RV	-	PR < 5%	-	PR < 5%	-	PR < 5%	-	-	-	-
60	RV	RV	PR < 5%	PR < 5%	PR < 5%	PR < 5%	PR < 5%	PR < 5%	PR < 5%	PR < 5%	PR < 5%
120	RV	-	PR < 5%	-	PR < 5%	-	PR < 5%	-	-	-	-

Table 2. Annealed microstructures and recrystallized volume fractions (V_V) for samples deformed to 47% reduction.

Time	Annealing temperature (°C)										
(min)	600	700	800	900	1000	1100	1200	1300	1350	1400	1450
2	RV	-	PR < 5%	-	PR 8 ± 3	-	PR 11 ± 3	-	-	-	-
5	RV	-	PR < 5%	-	PR 11 ± 4	-	PR 14 ± 5	-	-	-	-
10	RV	-	PR < 5%	-	PR 12 ± 5	-	PR 16 ± 4	-	-	-	-
15	RV	-	PR < 5%	-	PR 13 ± 4	-	PR 18 ± 7	-	-	-	-
30	RV	-	PR < 5%	-	PR 15 ± 5	-	PR 25 ± 8	-	-	-	-
45	RV	-	PR < 5%	-	PR 17 ± 7	-	PR 29 ± 9	-	-	-	-
		PR	PR	PR	PR	PR	PR	PR	PR	PR	PR

Table 3. Annealed microstructures and recrystallized volume fractions (V_V) for samples deformed to 61 % reduction.

Time	Annealing temperature (°C)										
(min)	600	700	800	900	1000	1100	1200	1300	1350	1400	1450
2	RV	-	PR < 5%	-	PR 12 ± 4	-	PR 15 ± 5	-	-	-	-
5	RV	-	PR < 5%	-	PR 15 ± 6	-	PR 19 ± 7	-	-	-	-
10	RV	-	PR < 5%	-	PR 17 ± 5	-	PR 24 ± 8	-	-	-	-
15	RV	-	PR < 5%	-	PR 21 ± 5	-	PR 26 ± 10	-	-	-	-
30	RV	-	PR < 5%	-	PR 25 ± 7	-	PR 31 ± 11	-	-	-	-
45	RV	-	PR 6 ± 2	-	PR 26 ± 8	-	PR 35 ± 8	-	-	-	-
60	RV	PR < 5%	PR 7 ± 3	PR 15 ± 6	PR 30 ± 8	PR 33 ± 7	PR 41 ± 9	PR 46 ± 13	PR 50 ± 17	PR 56 ± 18	PR 65 ± 20
120	RV	-	PR 9 ± 3	-	PR 32 ± 9	-	PR 44 ± 10	-	-	-	-

Table 4. Annealed microstructures and recrystallized volume fractions (V_V) for samples deformed to 72 % reduction.

Time	Annealing temperature (°C)										
(min)	600	700	800	900	1000	1100	1200	1300	1350	1400	1450
2	RV	-	PR < 5%	-	PR 18 ± 7	-	PR 21 ± 7	-	-	-	-
5	RV	-	PR < 5%	-	PR 23 ± 8	-	PR 30 ± 11	-	-	-	-
10	RV	-	PR < 5%	-	PR 29 ± 11	-	PR 41 ± 12	-	-	-	-
15	RV	-	PR < 5%	-	PR 35 ± 13	-	PR 57 ± 18	-	-	-	-
30	RV	-	PR 9 ± 4	-	PR 38 ± 14	-	PR 63 ± 17	-	-	-	-
45	RV	-	PR 11 ± 3	-	PR 44 ± 17	-	PR 68 ± 21	-	-	-	-
60	RV	PR < 5%	PR 12 ± 3	PR 21 ± 9	PR 46 ± 22	PR 55 ± 22	PR 71 ± 21	PR 79 ± 16	PR 83 ± 12	TR 91 ± 8	TR 95 ± 3
120	RV	-	PR 13 ± 4	-	PR 51 ± 19	-	PR 79 ± 16	-	-	-	-

heterogeneous in terms of grain size and morphology, as clearly shown in **Fig. 7**. Figure 7(b) shows a good example of the coexistence of recrystallized grains and "recovered" regions (bottom left part) in a sample deformed to 72 % and further annealed at 1 400°C for 1 h. A closer inspection reveals the presence of three types of grain morphologies in the recrystallized microstructure: 1) equiaxed grains resulting from the nucleation within wavy bands (former curly grain structure); 2) equiaxed grains confined within deformation bands; and 3) elongated grains confined within deformation bands (noticeable orientation pinning). There is a strong predominance of morphology of type 2 in our samples. Morphologies of type 1 and 2 occur preferentially in the central region of the samples. Grain size was about 20 μm in the equiaxed regions. The morphology of type 3 is often found at the edge of the bar and these elongated grains have a grain aspect ratio (GAR) above 10. **Figure 8** brings details of each one of the three different grain morphologies above described.

3.3. Recrystallization Kinetics

As a first approach, the recrystallization kinetics of a deformed metal can be studied using the well-known JMAK equation. The dependence of the transformed fraction with time is given as follows:

$$V_V = 1 - \exp(-Kt^n) \quad (1)$$

where V_V is the recrystallized volume fraction, t is the annealing time and K and n are constants. This model assumes that nuclei are randomly dispersed and the rates of nucleation and growth remain constant during annealing. Plotting $\ln\{\ln[1/(1-V_V)]\}$ *versus* $\ln t$ one can get the values of the Avrami exponents (n) for a set of samples deformed to 47, 61, and 72 % reduction and annealed at 1 000°C and 1 200°C from 2 to 120 min. These results are shown in **Fig. 9**. The Avrami exponents varied from 0.26 to 0.48. Admitting site-saturation nucleation, one expects values of n close to 3. Humphreys and Hatherly[8] hold that the deviation of recrystallization kinetics from the ideal linear JMAK plots and the low values of the Avrami exponent found in many experimental investigations, are in most cases directly attributable to the inhomogeneous distribution of stored energy. This leads to non-random distribution of nucleation sites and to a growth rate that decreases with time.[9] Furthermore, the stored energy per unit volume of unrecrystallized material is steadily reduced due to competing recovery processes, which retards recrystallization.[10] The extent of this effect depends on the material (specially its stacking fault energy), the amount of deformation, the annealing temperature and the heating rate. Competition between recovery and primary recrystallization is common-

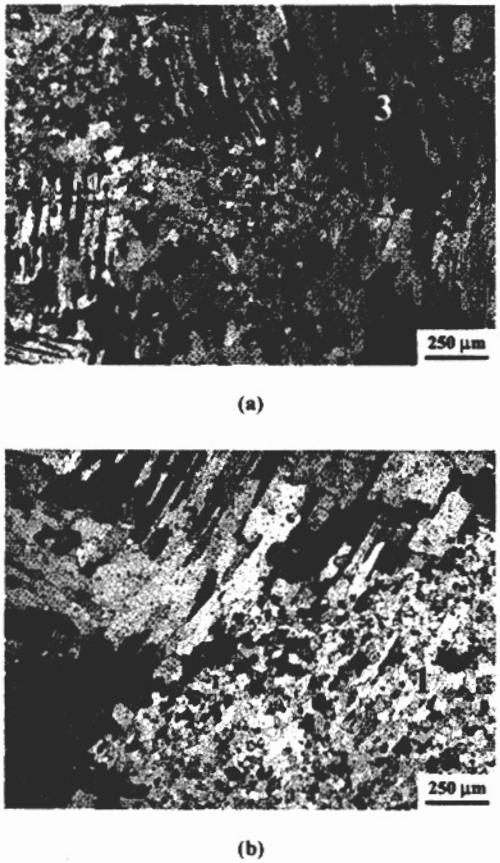

Fig. 7. Light optical micrographs showing the different grain morphologies found in recrystallized regions: a) sample deformed to 72% reduction and annealed at 1 450°C for 1 h; b) sample deformed to 72% reduction and annealed at 1 400°C for 1 h.

growth rate of the new grains was found to decrease with time in cold-rolled copper, for example. This behavior was attributed to the inhomogeneity of the stored energy distribution.[19]

In dispersion-containing alloys, there are at least two factors, acting in opposition, that influence the growth speed of the recrystallized regions. At one side, there is the stored energy due to the elastic energy of stored dislocations, driving force for primary recrystallization, to which the growth rate is directly proportional. On the other hand, we have the resistance pinning effect imposed by particles to the grain boundary migration, making it sluggish. The driving force for recrystallization is proportional to the dislocation density in the material, which depends on not only the particle volume fraction but also their size. The grain boundary pinning force due to particles (Zener drag) is directly proportional to the particle volume fraction and inversely proportional to the particle radius. The growth velocity depends on the balance between these two factors; in extreme cases, the resistance imposed by particles might stop boundary migration.

The results of electron metallography allow us interpreting the microstructure found in the annealed specimens. It can be explained as follows. Discontinuous recrystallization and extended recovery are responsible for the softening of

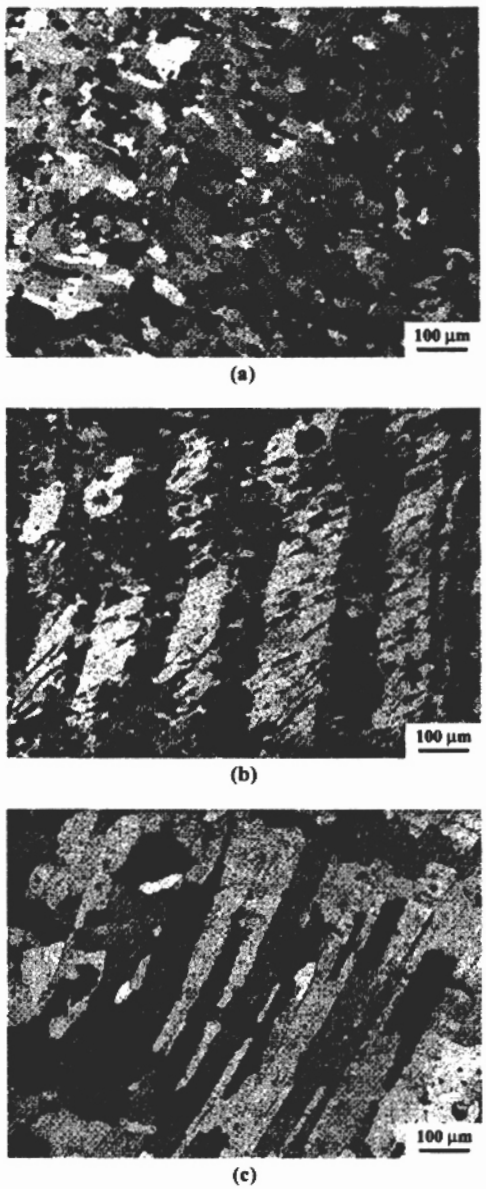

Fig. 8. Light optical micrographs of a sample deformed to 72% reduction and annealed at 1 450°C for 1 h showing details of the different grain morphologies observed in recrystallized regions: a) type 1; b) type 2; c) type 3.

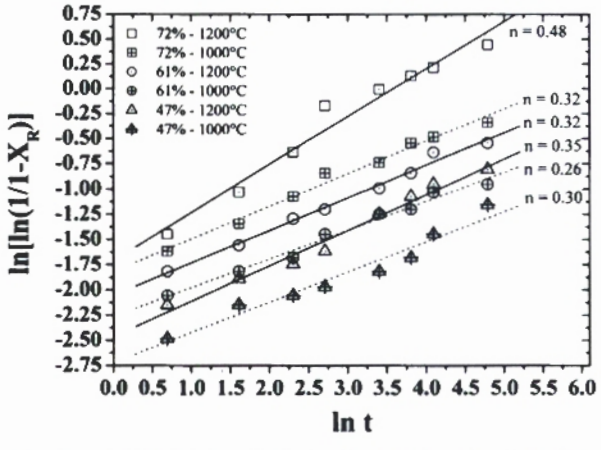

Fig. 9. JMAK plots (double log) of recrystallized volume frac-

within deformation heterogeneities. This behavior is explained mainly to the presence of larger curvatures as well as higher stored energies found at these regions. Nevertheless, in the regions where large grains are not present the microstructure consists of a particle-stabilized subgrain structure (typically found in materials softened by extended recovery) coexisting with small grains that could not overcome pinning effects. Why Zener pinning prevails in this case? One plausible explanation might be the absence of large misorientations surrounding these grains and because of the concurrent action of recovery decreasing the driving force locally. Similar findings were reported for other ODS superalloys like PM-1000,*2 a nickel-based dispersion-strengthened alloy with similar starting microstructure.[20]

3.4. EBSD Mappings

The microstructural characterization of annealed samples using EBSD reveals many interesting aspects concerning the recrystallization of this alloy. Compared to TEM, larger areas can be mapped using the EBSD technique providing detailed information on the microtexture and on the nature of boundaries developed upon annealing. Furthermore, the preparation of samples for EBSD is easier and faster. EBSD mappings could not be performed in most deformed specimens (>47% reduction) because of intrinsic limitation of the technique. Due to the large elastic energy stored in the deformed state, only weak-to-diffuse Kikuchi patterns could be acquired making impossible their indexing by using proper analysis software.

There are two important remarks concerning recrystallization in this ODS superalloy. First, nucleation of recrystallization is favored at deformation heterogeneities. The new grains visible in the light optical microscope were able to overcome pinning effects growing towards the substructure. **Figure 10** shows new recrystallized grains clustered at deformation heterogeneities. Details of the mesotexture found in this region are shown in the orientation map (Fig. 10(a)). Only boundaries with misorientations higher than 2° are indicated revealing the presence of a fairly organized subgrain structure. Most mapped points could be indexed because of the positive effect of recovery on sharpening of Kikuchi patterns. In the upper part of the orientation map it is possible identifying very small grains sizing less than 2 μm. A similar feature is depicted in **Fig. 11**. It shows the results of EBSD corresponding to a sample deformed to a larger strain and annealed at 1 350°C for 1 h. The orientation map of Fig. 11(a) shows a few recrystallized grains and a large recovered area in the surroundings. Another interesting feature is the presence of a deformation band in the central part of the map and a few small grains within it. It must be noted that most of the lines representing low angle boundaries in both maps are discontinuous. It means that some Kikuchi patterns could not be properly indexed because of lattice distortions or due to the presence of higher dislocation densities surrounding particles.

Another interesting feature associated to recrystallization in this ODS superalloy is the inhomogeneous in-grain and grain-to-grain spatial distributions of textures. It varies sig-

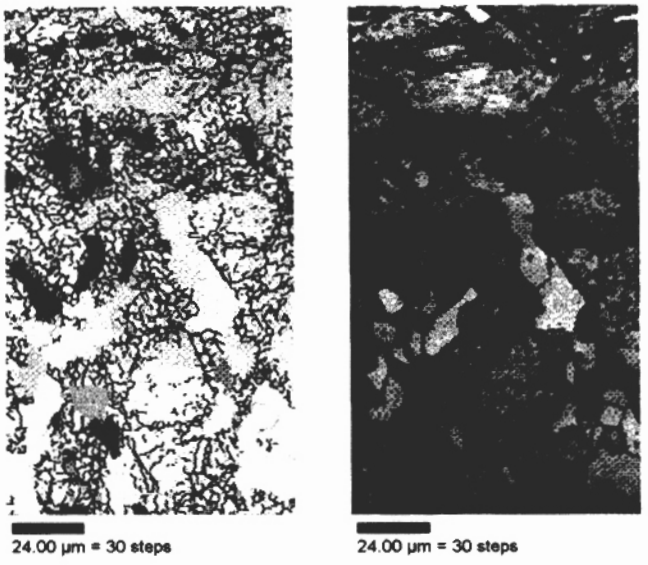

Fig. 10. EBSD mapping of a sample deformed to 61% reduction and annealed at 1 000°C for 2 h: a) OIM depicting new recrystallized grains clustered along deformation heterogeneities; b) IQ map.

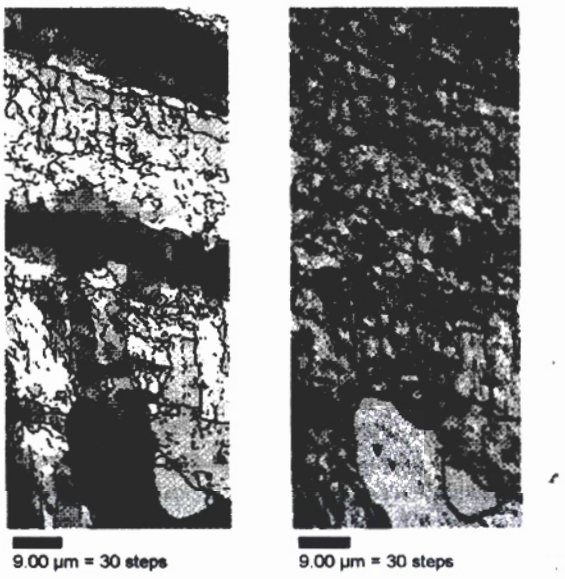

Fig. 11. EBSD mapping of a sample deformed to 72% reduction and annealed at 1 350°C for 1 h: a) OIM showing a few recrystallized grains (lower part) and a large recovered area in the surroundings; b) IQ map.

entation effects. **Figure 12**(a) shows the orientation map of a specimen deformed to 72% reduction and annealed at 1 450°C for 1 h. Recrystallization is not complete in the mapped region. Only recrystallized grains are show in this map. For purposes of presentation, the surrounding substructure was subtracted in this orientation map (black areas). The inverse pole figure (Fig. 12(b)) corresponding to the fine equiaxed grain structure shown in the bottom of the orientation map (type 1 morphology) indicates the existence of a nearly random texture. Contrastingly, the elon-

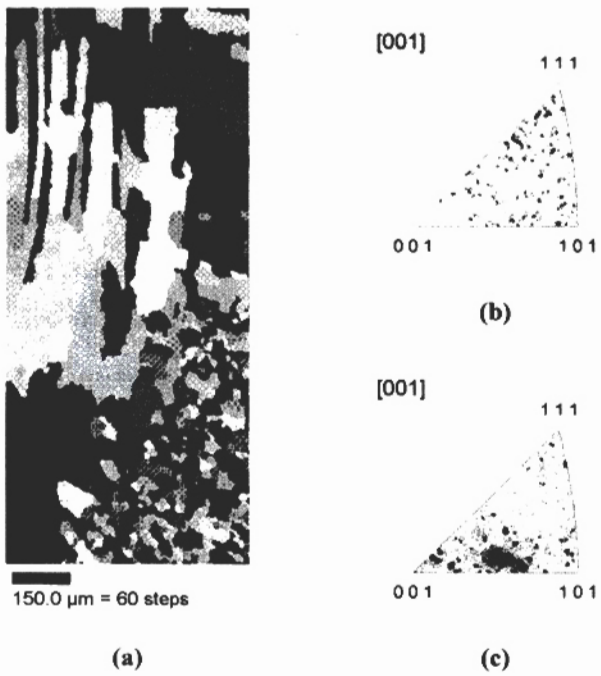

Fig. 12. EBSD mapping of a sample deformed to 72% reduction and annealed at 1 450°C for 1 h: a) OIM showing distinct recrystallized regions; b) inverse pole figure corresponding to the elongated grain structure; c) inverse pole figure corresponding to the fine equiaxed grain structure.

⟨102⟩ texture, as shown in Fig. 12(c).

3.5. Recrystallization Texture

The recrystallization texture was studied by the X-ray diffraction technique. The (110) and (200) pole figures were recorded in a texture goniometer for the sample deformed to 72% reduction and annealed at 1 450°C for 1 h. This sample was chosen because of its large recrystallized volume fraction (V_V>95%). As described in Part I, the ⟨111⟩-fiber texture found in the starting material has evolved towards a sharp ⟨110⟩-fiber texture during cold swaging. Results show that recrystallization did not change the texture significantly, as demonstrated in the (110)- and (200)-pole figures shown in **Fig. 13**. The maximum orientation density (TR, times random) of the (110) poles was TR=18.9.

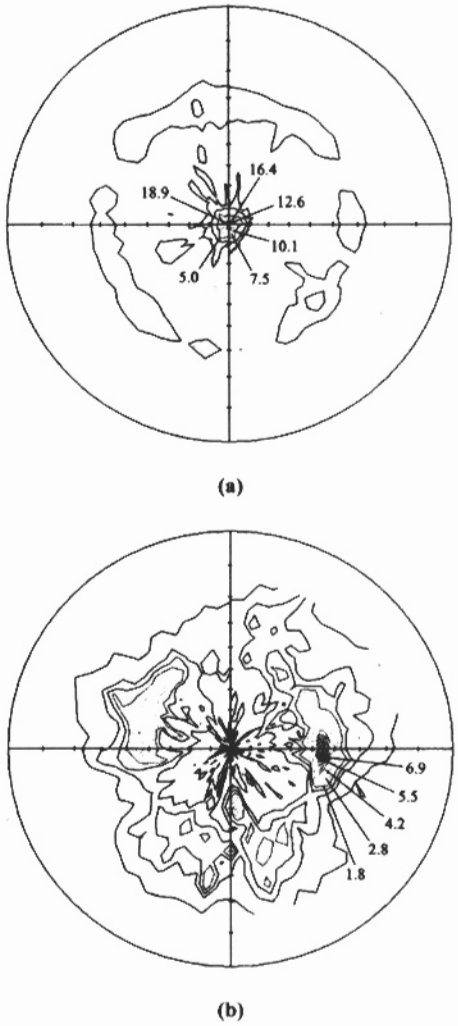

Fig. 13. Texture of sample deformed to 72% reduction and annealed at 1 450°C for 1 h: a) (110)-pole figure; b) (200)-pole figure.

4. Conclusions

Based on the microstructural evidences presented in this paper, the following conclusions are drawn:

(1) The annealing behavior of the MA 956 superalloy deformed by cold swaging has been systematically investigated. The balance between driving and dragging forces determine the final microstructure of this superalloy upon annealing. Recrystallized volume fractions $V_v \geq 70\%$ were evidenced in samples deformed at reductions higher than 60% and further annealed at temperatures above 1 200°C (this corresponds to a homologue temperature of 0.8 T_m).

(2) In the less deformed specimens, recrystallization was annealed at lower temperatures. Pinning of subgrain boundaries by particles have been revealed by TEM. This microstructure is representative of materials that have undergone extended recovery.

(3) The Johnson-Mehl-Avrami-Kolmogorov (JMAK) equation was used to test our experimental data. The Avrami exponents varied from 0.26 to 0.48 and are substantially smaller than those predicted theoretically. Concurrent recovery and a non-random distribution of recrystallization nuclei might explain this discrepancy.

(4) Discontinuous recrystallization and extended recovery are mostly responsible for the softening of this alloy. The large grains found in annealed specimens correspond to those were able to overcome Zener pinning. Nucleation of these large grains is favored in grain boundary regions and within deformation heterogeneities. This behavior is explained by the presence of larger curvatures as well as larger stored energies found at these regions. In regions where the large grains are not present the microstructure consists of a particle-stabilized subgrain structure coexisting with small grains whose growth was prevented by pinning effects.

for supporting this work (Grants No. 99/10793-8 and 99/06458-0). M. F. Hupalo acknowledges FAPESP for his Post-Doctoral scholarship under Contract No. 03/04046-3. Thanks are also due to Professor W. K. Reick (Ruhr-Universitat Bochum, Germany) for supplying the MA 956 alloy bars. H. R. Z. Sandim is CNPq fellow under Contract No. 300.158/02-5.

REFERENCES

1) T. S. Chou and H. K. D. H. Bhadeshia: *Mater. Sci. Technol.*, **9** (1993), 890.
2) W. Sha and H. K. D. H. Bhadeshia: *Metall. Trans. A*, **25A** (1994), 705.
3) W. Sha and H. K. D. H. Bhadeshia: *J. Mater. Sci.*, **30** (1995), 1439.
4) R. D. Klug, G. Krauss and D. K. Matlock: *Metall. Trans. A*, **27A** (1996), 1945.
5) T. S. Chou: *Mater. Sci. Eng. A*, **A223** (1997), 78.
6) G. Petzow: Metallographic Etching, ASM International, Metals Park, Ohio, (1978), 131.
7) A. Belyakov, Y. Sakai, T. Hara, Y. Kimura and K. Tsuzaki: *Scr. Mater.*, **48** (2003), 1463.
8) F. J. Humphreys and M. Hatherly: Recrystallization and Related Annealing Phenomena, Pergamon, Oxford, (1995), 203.
9) P. R. Rios: *Metall. Trans. A*, **28A** (1997), 939.
10) H. P. Stüwe, A. F. Padilha and F. Siciliano, Jr.: *Mater. Sci. Eng. A*, **A333** (2002), 361.
11) E. C. W. Perryman: *Trans. AIME J. Metals*, **203** (1955), 1053.
12) R. A. Vandermeer and P. Gordon: Recovery and Recrystallization of Metals, ed. by L. Himmel, Interscience, New York, (1963), 211.
13) H. P. Leighly Jr., F. C. Perkins and R. A. McCune: *J. Inst. Metals*, **92** (1963–64), 363.
14) D. Nobili, F. Mezzetti and E. Susi De Maria: *J. Mater. Sci.*, **3** (1968), 282.
15) F. C. Pimenta Jr., A. C. F. Arruda and A. F. Padilha: *Z. Metallkd.*, **77** (1986), 522.
16) E. A. Simielli, R. L. Plaut and A. F. Padilha: *Z. Metallkd.*, **78** (1987), 770.
17) A. Rosen, M. S. Burton and G. V. Smith: *Trans. Am. Inst. min. Eng.*, **230** (1964) 205.
18) F. Siciliano, Jr. and A. F. Padilha: *Z. Metallkd.*, **86** (1995), 713.
19) B. Hutchinson, S. Jonsson and L. Ryde: *Scr. Metall.*, **23** (1989), 671.
20) A. O. F. Hayama, H. R. Z. Sandim, J. F. C. Lins, M. F. Hupalo and A. F. Padilha: *Mater. Sci. Eng. A*, **A371** (2003), 198.